Journal of Materials Chemistry A

ROYAL SOCIETY OF CHEMISTRY

PAPER

View Article Online
View Journal | View Issue

Cite this: J. Mater. Chem. A, 2022, 10, 25595

An over 16% efficiency organic solar cell enabled by a low-cost pyrazine-based polymer donor†

Junzhen Ren,[ac] Shaoqing Zhang, *[b] Pengqing Bi,[a] Zhihao Chen,[a] Tao Zhang,[ac] Jingwen Wang,[ac] Lijiao Ma,[a] Jiayao Li[ac] and Jianhui Hou *[a]

Received 15th September 2022
Accepted 15th November 2022

DOI: 10.1039/d2ta07249a

rsc.li/materials-a

Developing organic photoactive materials with simple chemical structures is a promising strategy to solve the critical cost issue of organic solar cells (OSCs). Here, two pyrazine-based polymer donors with completely non-fused conjugated backbones, named PPz and PPz-T, are designed, synthesized and characterized for application in OSCs. The materials-only costs (MOCs) of both polymers are much lower than those of the current high-performance polymer donors. The temperature-dependent hole mobilities and optical absorption measurements reveal that PPz-T shows lower energy disorder and stronger pre-aggregation behavior than PPz. Moreover, more efficient exciton dissociation between PPz-T and BTP-eC9 occurs because of the matched highest occupied molecular orbital (HOMO) level. Finally, the optimal PPz-T:BTP-eC9-based device delivers a high power conversion efficiency (PCE) of 16.16%, which is one of the highest PCEs achieved in OSCs based on low-cost polymer donors. This work demonstrates that desirable PCE approaching state-of-the-art values can be achieved using newly designed low-cost polymers.

1 Introduction

Organic solar cells (OSCs) have attracted much attention due to their typical characteristics of light weight, flexibility, large-area fabrication and so on.[1–3] Benefitting from the rapid development of novel photovoltaic materials and device engineering in the last few years, the power conversion efficiencies (PCEs) of OSCs have currently reached over 19% for single-junction cells, demonstrating their great potential in future applications.[4–7] Such high performances are generally based on photovoltaic materials with complicated fused-ring chemical structures, *i.e.*, the star polymer donor PBDB-TF (PM6),[8] the non-fullerene acceptor Y6 (ref. 9) and their derivatives.[10–12] Meanwhile, the complex aromatic cyclization or fluorination reactions of the above-mentioned materials with state-of-the-art PCEs, such as fluorinated 2D-conjugated benzo[1,2-*b*:4,5-*b*′]dithiophene (BDT)[8] and alkylthiophene linked DTBT,[13] may thereby obstruct their future commercialization due to the cost issue. To reduce the synthetic cost, some efforts have been made to shorten synthesis steps,[14,15] employ simplified building block units,[16–18] or control reaction conditions and simplify purification methods,[19] among which designing novel photovoltaic materials with non-fused-ring chemical structures and without any expensive functional groups has been considered as an effective way to solve the critical cost issue.

Currently, the rational design of polymer donors with very simple chemical structures is mainly based on traditional conjugated polymers such as polythiophenes (PTs) and poly(-thiophene vinylene)s (PTVs), which show highly tunable optical and electronical properties and relatively efficient charge transport capabilities.[16,20–23] For instance, by systematically investigating the effect of miscibility between PDCBT-Cl and a series of non-fullerene acceptors (NFAs) on morphology and device performance, Ye *et al.* reported a high PCE of over 12% in PT-based OSCs.[24] Recently, Duan and co-workers demonstrated that new PT polymers with deep-lying energy levels as well as favorable packing properties can be achieved by introducing cyano-groups on the conjugated backbones, and the PT-derivatives, P5TCN-2F and P5TCN-F25, were successively reported with remarkable PCEs of 16.1% and 16.6% when blending with Y6 as the photoactive layer.[20,25] By introducing symmetrical ester groups at the β-position of thiophene units of (*E*)-1,2-di(thiophen-2-yl)ethene (TVT), we synthesized the poly(-thiophene vinylene) derivative PTVT-T that featured a stable planar molecular conformation and suitable aggregation behavior, and a high PCE of 16.2% was then realized.[16]Although photovoltaic performances based on low-cost polymers have approached those of state-of-the-art counterparts, there is difficulty in further efficiency improvement of the current

[a]State Key Laboratory of Polymer Physics and Chemistry, Beijing National Laboratory for Molecular Sciences, CAS Research/Education Center for Excellence in Molecular Sciences, Institute of Chemistry, Chinese Academy of Sciences, Beijing 100190, P. R. China. E-mail: hjhzlz@iccas.ac.cn

[b]School of Chemistry and Biological Engineering, University of Science and Technology Beijing, Beijing 100083, P. R. China. E-mail: shaoqingz@iccas.ac.cn

[c]University of Chinese Academy of Sciences, Beijing 100049, P. R. China

† Electronic supplementary information (ESI) available. See DOI: https://doi.org/10.1039/d2ta07249a

polymers with simple chemical structures, such as PTs and PTVs, due to the limitation of substitution positions along with the simplification of their conjugated backbones. Therefore, it is necessary to develop low-cost polymer donors that are constructed with new conjugated units in the backbones, providing more possibilities for realizing high PCE and low cost simultaneously.

Nitrogenous heterocyclic rings, including thiazole, pyrazine, pyridine, triazine, *etc.*, are widely used in organic photovoltaic, luminescence, fluorescent probe and other fields,[26–28] and among them, pyrazine derivatives, quinoxaline (Qx) and dithieno[3,2-*f*:2′,3′-*h*]quinoxaline (DTQx), have been successfully applied in OSCs due to their excellent electroluminescence properties.[29–31] The pyrazine unit, a building block widely available in the market, possesses a highly planar and symmetric geometry and electron-deficient nitrogen atoms at 1,4-positions. These characteristics are conducive to not only enhancing intermolecular interaction, but also strengthening intramolecular charge transfer (ICT), so as to synergistically modulate the energy levels, absorption spectra and pre-aggregation behavior of the corresponding polymers.[32] However, there is very little research on the use of the pyrazine unit in OSCs.[32–34]

Herein, we utilized low-cost pyrazine to design and synthesize a pair of polymers PPz and PPz-T, and investigate their differences in optical absorption, energy levels, pre-aggregation behaviours, photovoltaic performance, blend morphology, *etc.* Materials-only cost (MOC) analysis revealed considerably low synthesis cost for both polymers with few synthetic steps. Theoretical calculation showed that the non-covalent interaction induced by the nitrogen atoms of pyrazine can facilitate planar molecular skeletons and reduce the number of possible meta-conformations. The temperature-dependent hole mobilities and optical absorption measurements showed stronger aggregation behaviour and lower energy disorder in the PPz-T pristine film than in PPz. The electron-deficient feature of the nitrogen atom provides the two polymers with deep highest occupied molecular orbital (HOMO) levels, where PPz-T showed matched energy levels with the electron acceptor BTP-eC9 (abbreviated as eC9 in this contribution) to provide enough driving force for excitation separation. The optimal PPz-T:eC9-based device delivered a high PCE of 16.16%, which is among the highest performances based on low-cost polymer donors.

2 Results and discussion

2.1 Material synthesis and characterization

The synthetic route as well as the chemical structures of the two polymers, PPz and PPz-T, are shown in Fig. 1a, and detailed synthesis procedures are provided in the ESI.† To balance the solubility and aggregation behaviour of the polymers, 3-butylnonyl chains are specially chosen as side chains. Compound **1** was synthesized according to the reported work.[35] Compound **2** was obtained by brominating compound **1** with NBS as the bromination agent, and then a nucleophilic substitution reaction was carried out to produce compound **3**. Subsequently, compound **4** was synthesized through coupling 2,5-dibromopyrazine with compound **3**, so as to produce organotin monomer **5** and brominated monomer **6**. Finally, target polymer PPz was obtained through polymerization between monomers **5** and **6**, and PPz-T was obtained by polymerization between monomer **6** and the 2,5-bis(trimethylstannyl)thiophene unit. The synthesis costs of PPz and PPz-T were evaluated based on the MOC method proposed in our previous work,[16] and the detailed analysis standards are listed in Tables S1 and S2.† PPz and PPz-T show a low MOC of 34.59 and 30.17 $ per g, respectively, which are at the same level as those of PTVT-T and PTVT-BT, the low-cost polymers we have developed before, and lower than those of other polymers with PCEs over 16% (Fig. 2f).[16,36] The two polymers showed good solubility in chloroform, toluene, *o*-xylene, chlorobenzene and other commonly used solvents in the OSC fabrication process. The number average molar mass (M_n) and polydispersity index ($Đ$) of PPz and PPz-T were measured by gel permeation chromatography with trichlorobenzene as

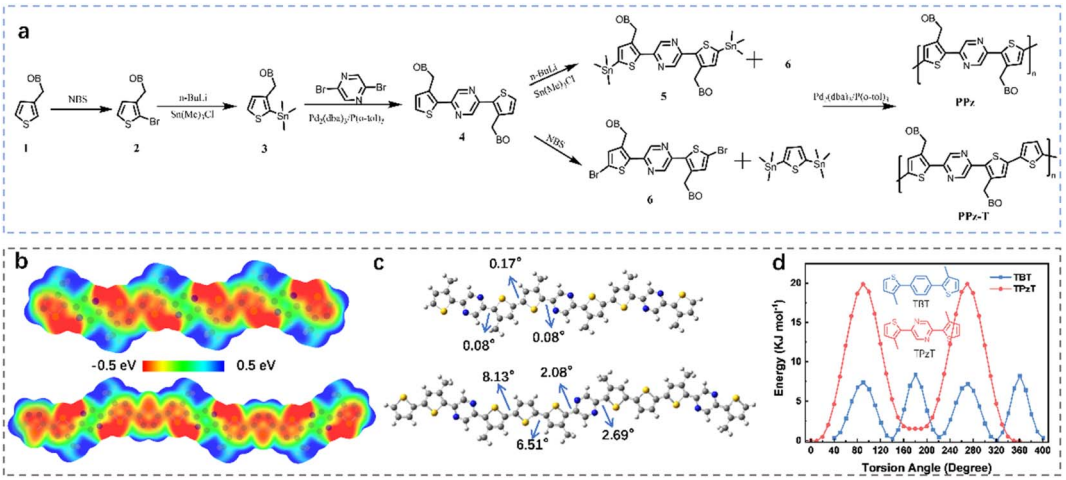

Fig. 1 (a) Molecular structures and corresponding synthetic routes of PPz and PPz-T; (b) theoretical calculation at the B3LYP/6-31G(d,p) level: ESP distribution and (c) calculated molecular geometries and corresponding dihedral angles of PPz and PPz-T trimers; (d) torsional energy profiles between thiophene and pyrazine of the TPzT model, and thiophene and benzene of the TBT model.

solvent at 145 °C, which are 68 kDa with a $Đ$ of 2.7 and 55 kDa with a $Đ$ of 2.5, respectively. Thermogravimetric analysis (TGA) was conducted to measure the thermal decomposition temperature (T_d) of PPz and PPz-T, and as depicted in Fig. S1,† the T_ds are 378 and 435 °C, respectively, indicating their good thermal stability for device fabrication.

2.2 Theoretical calculation

To investigate the electronic distribution and molecular conformations of the two polymers, density functional theory (DFT) calculation was undertaken to optimize the conformations of the trimers of PPz and PPz-T for calculating the corresponding frontier molecular orbitals, surface electrostatic potential (ESP), dihedral angles and torsional energy. PPz and PPz-T trimers have similar electronic distribution of the HOMO and lowest unoccupied molecular orbital (LUMO) (Fig. S2†), and the calculated HOMO/LUMO levels are −4.95/−2.46 eV and −4.84/−2.50 eV for PPz and PPz-T, respectively. Both polymers have uniform ESP distribution as well as typical electron-donor characteristics (Fig. 1b), where negative electrostatic potentials are mainly around sulfur and nitrogen atoms. Additionally, the average ESP values of individual atoms were calculated using Multiwfn.[37] As shown in Fig. S3,† PPz-T exhibits a more obvious negative potential than PPz from the perspective of average ESP values of individual atoms, mainly because of more electron-rich thiophenes existing in the backbone of PPz-T. The dihedral angles of PPz between pyrazine and thiophene, thiophene and thiophene, are about 0.34° and 0.26°, respectively, which indicates a planar backbone in PPz that may result from the strong noncovalent interaction between nitrogen atoms and sulfur atoms. When inserting a thiophene unit into the backbone to construct PPz-T, as displayed in Fig. 1c, the dihedral angles between pyrazine and thiophene, thiophene and thiophene in PPz-T rise to 2.69° and 8.13°, respectively, which may be attributed to the relatively weakened S···H noncovalent interaction between the inserted thiophene and adjacent alkyl thiophenes. To further explore the effect of the nitrogen atoms in the pyrazine unit on the molecular conformation of the polymers, energy curves *versus* torsion angle were also scanned by building two molecular models of thiophene–benzene–thiophene (TBT) and thiophene–pyrazine–thiophene (TPzT), and from the chart depicted in Fig. 1d, it is found that the TBT unit has four stable conformations with energy barriers of about 7.5 kJ mol^{-1} between each other, and each conformation is twisted with big dihedral angles of about 40°. Only one stable conformation and one meta-stable conformation exist in the TPzT unit, and the dihedral angles between thiophene and pyrazine of the stable conformation are about 0°, which implies a planar skeleton induced by intramolecular noncovalent interaction in the TPzT unit. The above results illustrate that PPz and PPz-T show a relatively planar molecular backbone, and pre-aggregation behavior induced by strong intermolecular interaction can be expected.

2.3 Optical and electrochemical properties

PPz and PPz-T present similar UV-vis absorption spectra in the film state with an absorption range of 400–600 nm in Fig. 2a, which is complementary to the light absorption of the non-fullerene acceptor eC9 in the visible region. Compared to PPz, the absorption peak and absorption edge of the PPz-T film are slightly red-shifted, which may be due to the enhanced ICT effect caused by the introduction of more electron-rich thiophenes in the backbone. The optical absorption gaps (E_g^{opt}) of PPz and PPz-T were calculated as 2.08 eV and 2.05 eV,

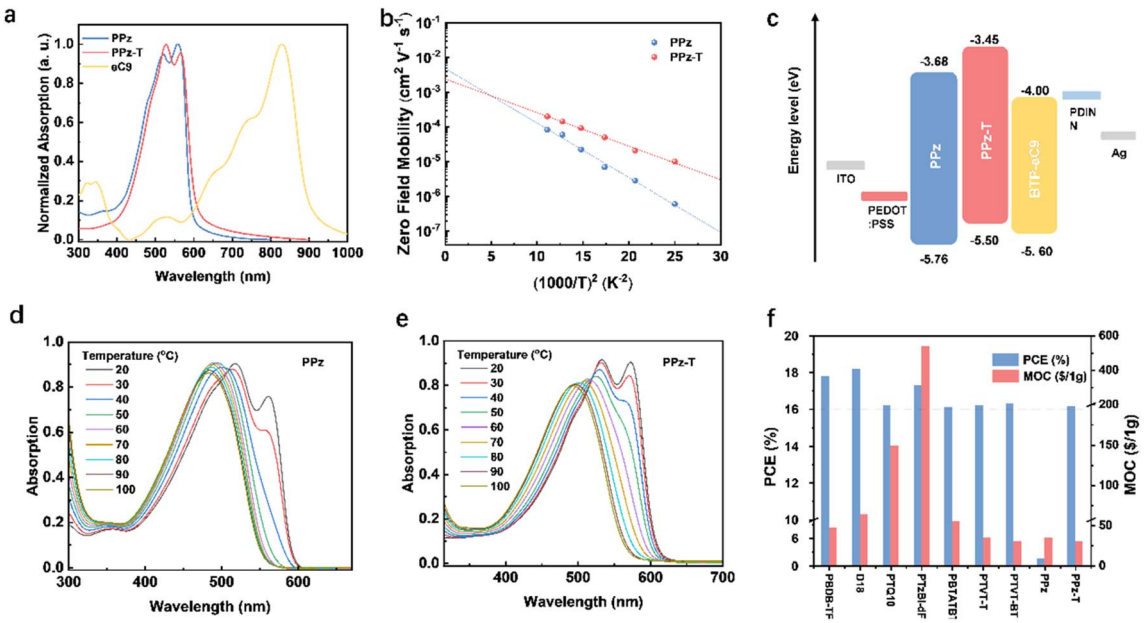

Fig. 2 (a) Optical absorption spectra of PPz, PPz-T and eC9 films; (b) hole mobilities of PPz and PPz-T films as a function of $1/T^2$ using SCLC derived data; (c) energy level alignment of PPz, PPz-T and eC9; (d and e) absorption spectra of PPz (d) and PPz-T (e) at varying temperature in chlorobenzene solution; (f) the MOC and PCE of several representative polymer donors with PCE over 16% and the polymers in this work.

respectively, which agree well with the theoretically calculated values aforementioned. To investigate the aggregation behavior of the two polymers in solution, temperature-dependent light absorption was measured from 20 °C to 100 °C and the corresponding profiles are shown in Fig. 2d and e. As is shown, the absorption profiles of both polymers are gradually blue-shifted while the vibration shoulder peaks weakened with the rise in temperature of the solution. When the temperature went up to 60 °C, the shoulder peak of PPz-T disappeared, which was obviously higher than that of the PPz solution (40 °C). In order to clarify the influence of molecular structure on the degree of energy disorder in the film state, the hole mobilities of the two polymers at different temperatures were measured by the SCLC method with a device structure of ITO/PEDOT:PSS/polymer/MoO_3/Au and the corresponding plots are shown in Fig. 2b. At room temperature, the hole mobility of PPz-T was 2.11×10^{-4} cm^{-2} V^{-1} S^{-1}, which was higher than that of PPz (8.10×10^{-5} cm^{-2} V^{-1} S^{-1}). Based on the Gaussian disorder model (GDM),[38,39] the electronic states of hole transport were further investigated, where the hole mobilities of both polymer films presented a downward trend as the temperature decreased, but the rate at which the hole mobility of PPz decreased was evidently larger than that of PPz-T. The energy disorder (σ) values were calculated as 78 and 61 meV, respectively, which implied that fewer trap states existed in the PPz-T film than PPz. The frontier molecular orbital energy levels of PPz and PPz-T as well as the electron-acceptor eC9 were measured by cyclic voltammetry with ferrocene as an internal standard. The relevant curves and energy level alignment are summarized in Fig. 2c and S4.† PPz showed a deep-lying HOMO level of −5.76 eV, and PPz-T presented a much higher HOMO level of −5.50 eV due to the introduction of the electron-rich thiophene unit in its backbone. It should be noticed that the HOMO level of PPz is even deeper than that of the electron acceptor eC9 (−5.60 eV), which implies insufficient driving force may occur in the PPz:eC9-based OSCs. The LUMO levels were calculated according to the formula $E_{LUMO} = E_g^{opt} - E_{HOMO}$, and the values for PPz and PPz-T are −3.68 eV and −3.45 eV, respectively.

2.4 Photovoltaic properties

To investigate the photovoltaic characteristics of PPz and PPz-T, OSCs were fabricated with a traditional structure of ITO/PEDOT:PSS/polymer:eC9/PDINN/Ag. The detailed device fabrication process is given in the ESI,† and the corresponding *J*–*V* curves and photovoltaic parameters are summarized in Fig. 3a and S5 as well as Table 1 and S3,† respectively. As shown in Fig. 3a, the optimal PPz:eC9-based device provided an unsatisfactory PCE of 1.40% with an open circuit voltage (V_{OC}) of 0.96 V, a short circuit current (J_{SC}) of 4.32 mA cm^{-2} and a fill factor (FF)

Table 1 Photovoltaic parameters for the polymer:eC9-based OSCs

Blends	V_{OC} (V)	J_{SC} (mA cm^{-2})	J_{cal}[a] (mA cm^{-2})	FF	PCE (%)
PPz:eC9	0.96	4.32	4.25	0.34	1.40
PPz-T:eC9	0.85	26.29	25.27	0.73	16.16

[a] Integrated from EQE curves.

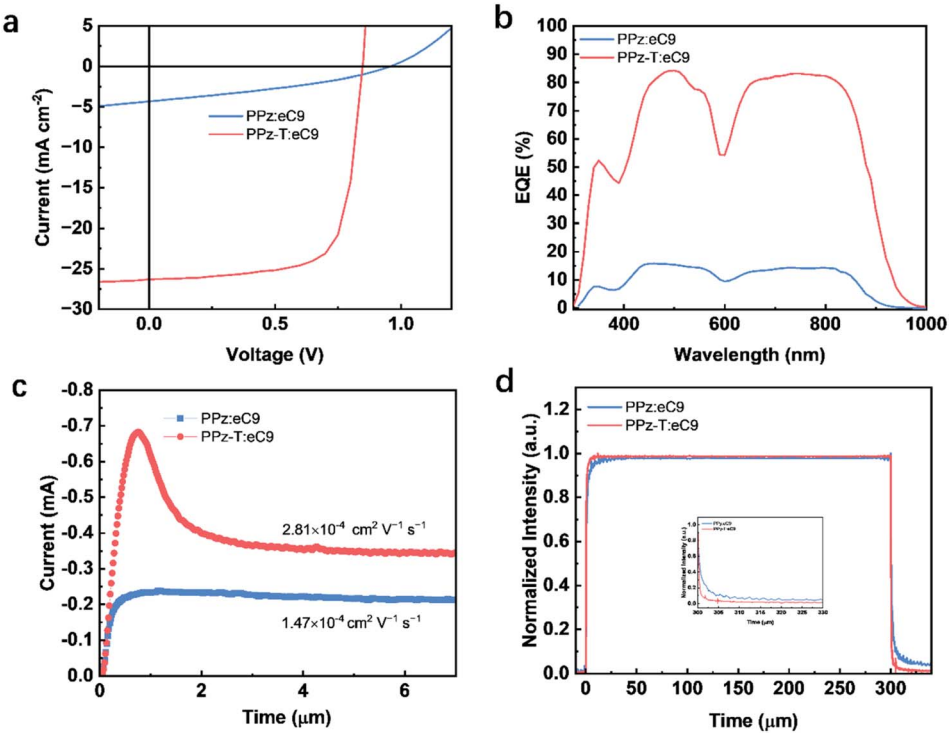

Fig. 3 Photovoltaic characteristics: the *J*–*V* curves (a), EQE responses (b), photo-CELIV curves (c), and transient photocurrent measurement (d) in response to a 300 μs white light (LED) pulse of PPz- and PPz-T-based devices.

of 0.34. Such low J_{SC} and FF values are ascribed to the ineffective hole transfer from eC9 to PPz induced by the mismatched HOMO levels between PPz and eC9 as indicated before. In contrast, the optimized device based on PPz-T:eC9 showed an excellent efficiency of 16.16% with a V_{OC} of 0.85 V, a J_{SC} of 26.29 mA cm^{-2} and a FF of 0.73. External quantum efficiency (EQE) measurements showed that the integrated current densities are 4.25 and 25.27 mA cm^{-2} for PPz:eC9- and PPz-T:eC9-based devices (Fig. 3b), respectively, which are consistent with the values obtained from *J–V* measurements. The charge mobilities of faster carriers were also measured through photoinduced charger-carrier extraction by linearly increasing the voltage (photo-CELIV) and the corresponding data are shown in Fig. 3c. The charge mobility of the PPz-T:eC9 film was 2.81×10^{-4} cm^{-2} V^{-1} S^{-1}, which is obviously higher than that of the PPz:eC9 film (1.47×10^{-4} cm^{-2} V^{-1} S^{-1}). The transient photocurrent was probed based on the turn-off dynamics in response to a 300 μs white light (LED) pulse, and Fig. 3d presents a faster turn-off character of PPz-T:eC9, which indicates fewer traps existing in the PPz-T:eC9 film.

2.5 Charge transfer analysis

The differences in photovoltaic parameters of the two devices are closely related to the charge generation, separation and recombination processes.[40,41] As the two blends possess sufficient ΔE_{LUMO} (D–A) for electron transfer, transient adsorption (TA) was used to study the hole generation and transfer processes here. An excitation wavelength of 800 nm was used to selectively excite the acceptor. The 2D TA images and the corresponding TA spectra with various decay times are shown in Fig. 4a–d. The TA signals in the ranges of 650–850 nm and 850–1000 nm correspond to the ground state bleaching (GSB) and excited state absorption (ESA) of eC9, respectively. The GSB signals of PPz-T are in the range of 450–580 nm and its ESA signals are in the range of 580–630 nm. When eC9 was excited, the response signals of PPz-T (GSB and ESA) appeared almost at the same time, which means very fast hole transfer from eC9 to PPz-T. The decay dynamics at 571 nm (corresponding to the GSB of PPz-T) and 731 nm (corresponding to the GSB of eC9) were investigated to clearly observe the hole transfer process. As depicted in Fig. 4e, with the quick signal decay of eC9, the response of PPz-T kept increasing until about 500 fs and then decayed, indicating a fast hole transfer process from eC9 to PPz-T. In contrast, no distinct hole transfer phenomenon could be observed in the PPz:eC9-based system (Fig. S6†), except for the simultaneously excited signals of eC9 located in the 450–510 nm and 530–630 nm ranges at 500 fs and 1 ps (Fig. 4f). This is mainly due to the insufficient driving force for hole separation in the PPz:eC9-based system. The results also showed that the photoelectron conversion efficiency of the PPz-T:eC9-based system was significantly higher than that of its PPz:eC9-based counterpart.

2.6 Morphology measurement

The morphological properties of the pristine polymers and blend films were then investigated using atomic force microscopy (AFM) and grazing-incidence wide-angle X-ray scattering (GIWAXS) measurements. As shown in Fig. 5a–h, the neat films of PPz and PPz-T showed a smooth film aggregation morphology with similar root mean square surface roughness (R_q) values (0.85 nm for PPz and 1.03 nm for PPz-T). When blending with eC9, a slightly rougher surface with R_q values of ~1.30 nm relative to the neat polymer films and obvious phase separation could be observed for the two blends. More

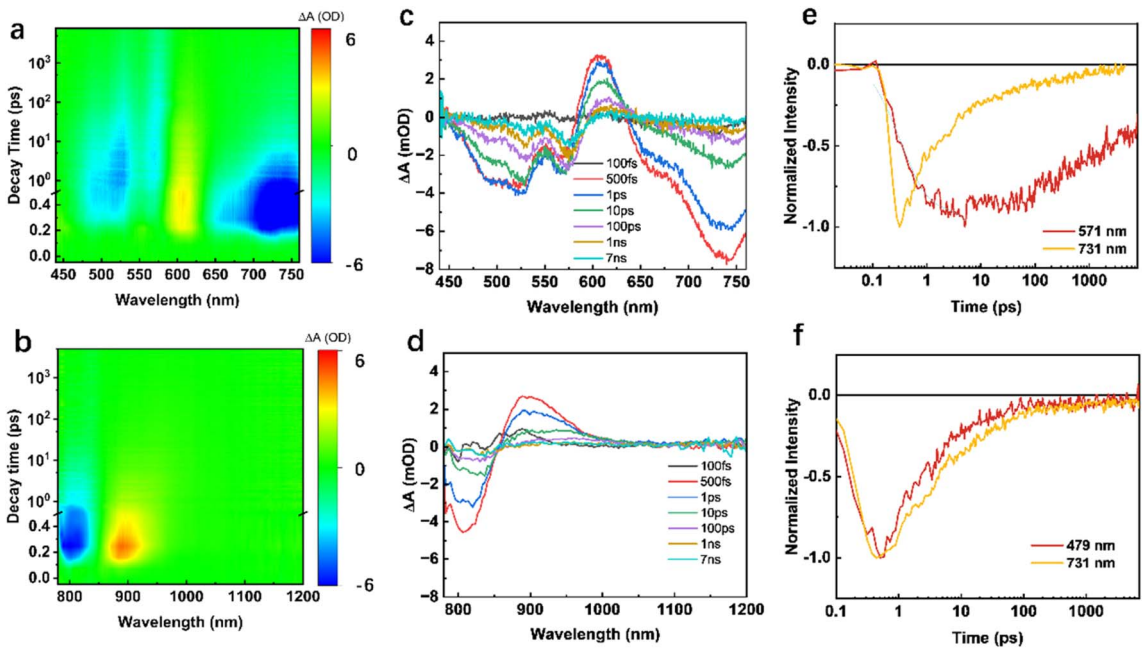

Fig. 4 (a and b) Color plot of 2D TA spectra of PPz-T:eC9 blends under 800 nm excitation. (c and d) TA spectra of PPz-T:eC9 blend at indicated delay times. (e and f) the decay dynamics of PPz-T:eC9 (e) and PPz:eC9 (f) at indicated wavelength.

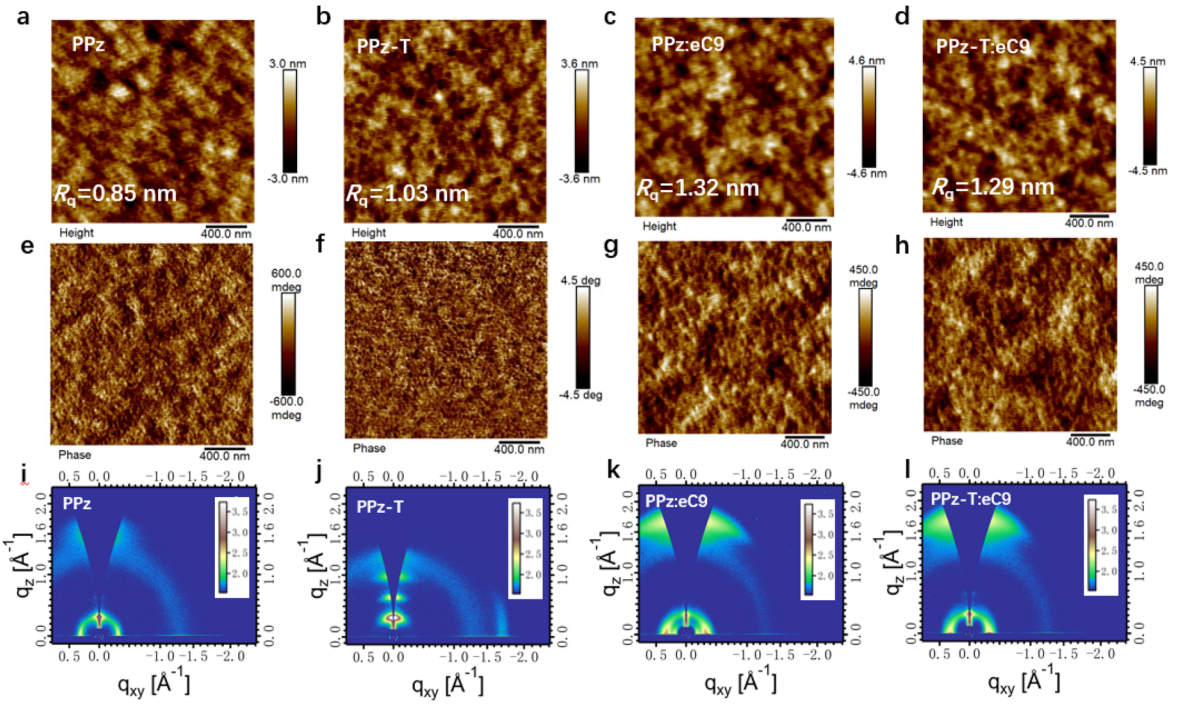

Fig. 5 (a–d) AFM height images and (e–h) phase images of PPz, PPz-T, and PPz:eC9 films, and the PPz-T:eC9 film. (i–l) 2D GIWAXS patterns of PPz, PPz-T, and PPz:eC9 films, and the PPz-T:eC9 film.

exploration of the neat and blend films was provided by GIWAXS measurements, and as indicated in Fig. 5i, l and S7,† the neat film of PPz presented a face-on orientation with representative face-on diffraction signals, (010) peak out of plane (1.54 Å^{-1}) and (100) peak in plane (0.32 Å^{-1}), corresponding to a π–π stacking distance of 4.08 Å and lamellar spacing of 19.63 Å, respectively. For the PPz-T neat film, no obvious (010) diffraction patterns in the out-of-plane direction could be observed, but there was a diffraction peak in plane at 1.72 Å^{-1} (corresponding to a π–π stacking distance of 3.65 Å) and a series of diffraction signals out of plane at 0.32, 0.65 and 0.97 Å^{-1} that represent (100), (200) and (300) peaks, respectively, all of which suggesting that the PPz-T film formed strong ordered intermolecular stacking along the edge-on orientation. Besides, we also investigated the GIWAXS of the electron-acceptor eC9, and as shown in Fig. S7a,† the eC9 film had obvious face-on stacking with a (010)-diffraction peak out of plane at 1.74 Å^{-1}. Both blend films of PPz:eC9 and PPz-T:eC9 showed typical face-on orientation with the same diffraction patterns with (100) peaks in plane and (010) peaks out of plane located at 0.32 Å^{-1} and 1.73 Å^{-1}, respectively. The (100) peaks in plane should originate from the aggregation behavior of the polymer donor (PPz and PPz-T) phase while the (010) peaks in the out-of-plane direction may be attributed to the intermolecular stacking of the eC9 phase. Interestingly, blending eC9 effectively induced the transformation of the molecular stacking direction from edge-on orientation of the PPz-T pure film to face-on orientation of the blend film, which contributed to efficient charge transportation along the vertical direction of the device.

3 Conclusions

In this work, two low-cost polymer donors, PPz and PPz-T, were designed and synthesized by employing the widely commercially available pyrazine unit. The materials-only cost (MOC) analysis revealed that both the polymers possess considerably low synthesis cost with few synthetic steps. PPz and PPz-T showed a stable planar conformation and strong aggregation behavior in solution, indicating their great potential in the formation of proper phase separation when blending with NFAs. Due to the deep-lying HOMO level of −5.76 eV for PPz, the PCE of the OSC based on PPz:eC9 was only 1.40% as there was insufficient driving force for charge separation in the blend. Encouragingly, the suitable offset between the HOMO levels of PPz-T and eC9 together with the favorable phase separation in the active layer led to a remarkable PCE over 16% in the PPz-T:eC9-based OSC, which is one of the highest values for devices based on low-cost polymer donors. This work not only introduced two low-cost polymers with very simple molecular backbones consisting of pyrazine units, but also demonstrates that desirable PCE approaching state-of-the-art values can be obtained by appropriate molecular design methods.

Conflicts of interest

There are no conflicts to declare.

Acknowledgements

This work was financially supported by the National Natural Science Foundation of China (21835006 and 22075017) and the

National Key Research and Development Program of China (2019YFE0116700).

Notes and references

1 L. Meng, Y. Zhang, X. Wan, C. Li, X. Zhang, Y. Wang, X. Ke, Z. Xiao, L. Ding, R. Xia, H.-L. Yip, Y. Cao and Y. Chen, *Science*, 2018, **361**, 1094–1098.
2 C. Yan, S. Barlow, Z. Wang, H. Yan, A. K. Y. Jen, S. R. Marder and X. Zhan, *Nat. Rev. Mater.*, 2018, **3**, 1–19.
3 J. Hou, O. Inganas, R. H. Friend and F. Gao, *Nat. Mater.*, 2018, **17**, 119–128.
4 L. Zhu, M. Zhang, J. Xu, C. Li, J. Yan, G. Zhou, W. Zhong, T. Hao, J. Song, X. Xue, Z. Zhou, R. Zeng, H. Zhu, C. C. Chen, R. C. I. MacKenzie, Y. Zou, J. Nelson, Y. Zhang, Y. Sun and F. Liu, *Nat. Mater.*, 2022, **21**, 656–663.
5 R. Ma, C. Yan, J. Yu, T. Liu, H. Liu, Y. Li, J. Chen, Z. Luo, B. Tang, X. Lu, G. Li and H. Yan, *ACS Energy Lett.*, 2022, **7**, 2547–2556.
6 C. He, Y. Pan, Y. Ouyang, Q. Shen, Y. Gao, K. Yan, J. Fang, Y. Chen, C.-Q. Ma, J. Min, C. Zhang, L. Zuo and H. Chen, *Energy Environ. Sci.*, 2022, **15**, 2537–2544.
7 Y. Wei, Z. Chen, G. Lu, N. Yu, C. Li, J. Gao, X. Gu, X. Hao, G. Lu, Z. Tang, J. Zhang, Z. Wei, X. Zhang and H. Huang, *Adv. Mater.*, 2022, **34**, e2204718.
8 M. Zhang, X. Guo, W. Ma, H. Ade and J. Hou, *Adv. Mater.*, 2015, **27**, 4655–4660.
9 J. Yuan, Y. Zhang, L. Zhou, G. Zhang, H.-L. Yip, T.-K. Lau, X. Lu, C. Zhu, H. Peng, P. A. Johnson, M. Leclerc, Y. Cao, J. Ulanski, Y. Li and Y. Zou, *Joule*, 2019, **3**, 1140–1151.
10 C. Li, J. Zhou, J. Song, J. Xu, H. Zhang, X. Zhang, J. Guo, L. Zhu, D. Wei, G. Han, J. Min, Y. Zhang, Z. Xie, Y. Yi, H. Yan, F. Gao, F. Liu and Y. Sun, *Nat. Energy*, 2021, **6**, 605–613.
11 X. Kong, C. Zhu, J. Zhang, L. Meng, S. Qin, J. Zhang, J. Li, Z. Wei and Y. Li, *Energy Environ. Sci.*, 2022, **15**, 2011–2020.
12 H. Chen, H. Liang, Z. Guo, Y. Zhu, Z. Zhang, Z. Li, X. Cao, H. Wang, W. Feng, Y. Zou, L. Meng, X. Xu, B. Kan, C. Li, Z. Yao, X. Wan, Z. Ma and Y. Chen, *Angew. Chem., Int. Ed.*, 2022, **134**, e202209580.
13 Q. Liu, Y. Jiang, K. Jin, J. Qin, J. Xu, W. Li, J. Xiong, J. Liu, Z. Xiao, K. Sun, S. Yang, X. Zhang and L. Ding, *Sci. Bull.*, 2020, **65**, 272–275.
14 X. Li, F. Pan, C. Sun, M. Zhang, Z. Wang, J. Du, J. Wang, M. Xiao, L. Xue, Z. G. Zhang, C. Zhang, F. Liu and Y. Li, *Nat. Commun.*, 2019, **10**, 519.
15 L. Li, F. Meng, M. Zhang, Z. G. Zhang and D. Zhao, *Angew. Chem., Int. Ed.*, 2022, **61**, e202206311.
16 J. Ren, P. Bi, J. Zhang, J. Liu, J. Wang, Y. Xu, Z. Wei, S. Zhang and J. Hou, *Natl. Sci. Rev.*, 2021, **8**, nwab031.
17 X. Wang, R. Zhao, Z. Ding, S. F. Liu and Y. Li, *Sci. China Chem.*, 2022, **65**, 1775–1781.
18 H. Ning, G. Zhang, H. Chen, Z. Wang, S. Ni, F. Lu, F. Liu, L. Dang, J. Liu, F. He and Q. Wu, *Chem. Mater.*, 2021, **33**, 1976–1982.
19 W. Liu, S. Xu, H. Lai, W. Liu, F. He and X. Zhu, *CCS Chem.*, 2022, DOI: **10.31635/ccschem.022.202201963**.
20 X. Yuan, Y. Zhao, D. Xie, L. Pan, X. Liu, C. Duan, F. Huang and Y. Cao, *Joule*, 2022, **6**, 647–661.
21 P. Bi, J. Ren, S. Zhang, J. Wang and J. Hou, *Polymer*, 2020, **209**, 122900.
22 D. Jeong, G. U. Kim, D. Lee, S. Seo, S. Lee, D. Han, H. Park, B. Ma, S. Cho and B. J. Kim, *Adv. Energy Mater.*, 2022, **12**, 2201603.
23 J. Xiao, X. Jia, C. Duan, F. Huang, H. L. Yip and Y. Cao, *Adv. Mater.*, 2021, **33**, e2008158.
24 Z. Liang, M. Li, Q. Wang, Y. Qin, S. J. Stuard, Z. Peng, Y. Deng, H. Ade, L. Ye and Y. Geng, *Joule*, 2020, **4**, 1278–1295.
25 X. Yuan, Y. Zhao, Y. Zhang, D. Xie, W. Deng, J. Li, H. Wu, C. Duan, F. Huang and Y. Cao, *Adv. Funct. Mater.*, 2022, **32**, 2201142.
26 D. Zhu, X. Bao, Q. Zhu, C. Gu, M. Qiu, S. Wen, J. Wang, B. Shahid and R. Yang, *Energy Environ. Sci.*, 2017, **10**, 614–620.
27 G. Zhang, H. Yu, M. Sun, L. Tang and L. Qiu, *Dyes Pigm.*, 2021, **194**, 109660.
28 W. Huang, J. Byun, I. Rorich, C. Ramanan, P. W. M. Blom, H. Lu, D. Wang, L. Caire da Silva, R. Li, L. Wang, K. Landfester and K. A. I. Zhang, *Angew. Chem., Int. Ed.*, 2018, **57**, 8316–8320.
29 S. Xu, X. Wang, L. Feng, Z. He, H. Peng, V. Cimrová, J. Yuan, Z.-G. Zhang, Y. Li and Y. Zou, *J. Mater. Chem. A*, 2018, **6**, 3074–3083.
30 Y. Xu, Y. Cui, H. Yao, T. Zhang, J. Zhang, L. Ma, J. Wang, Z. Wei and J. Hou, *Adv. Mater.*, 2021, **33**, e2101090.
31 C. Sun, F. Pan, H. Bin, J. Zhang, L. Xue, B. Qiu, Z. Wei, Z. G. Zhang and Y. Li, *Nat. Commun.*, 2018, **9**, 743.
32 J. Wu, Q. Fan, M. Xiong, Q. Wang, K. Chen, H. Liu, M. Gao, L. Ye, X. Guo, J. Fang, Q. Guo, W. Su, Z. Ma, Z. Tang, E. Wang, H. Ade and M. Zhang, *Nano Energy*, 2021, **82**, 105679.
33 L. Guo, K. Liu, X. Tan, X. Wang, J. Huang, Z. Wei and G. Chen, *Macromolecules*, 2021, **54**, 10758–10766.
34 L. Zhou, X. Xia, L. Meng, J. Zhang, X. Lu and Y. Li, *Chem. Mater.*, 2021, **33**, 8212–8222.
35 Z. Ou, J. Qin, K. Jin, J. Zhang, L. Zhang, C. Yi, Z. Jin, Q. Song, K. Sun, J. Yang, Z. Xiao and L. Ding, *J. Mater. Chem. A*, 2022, **10**, 3314–3320.
36 P. Bi, J. Ren, S. Zhang, J. Wang, Z. Chen, M. Gao, Y. Cui, T. Zhang, J. Qin, Z. Zheng, L. Ye, X. Hao and J. Hou, *Nano Energy*, 2022, **100**, 107463.
37 T. Lu and F. Chen, *J. Comput. Chem.*, 2012, **33**, 580–592.
38 J. Yuan, C. Zhang, B. Qiu, W. Liu, S. K. So, M. Mainville, M. Leclerc, S. Shoaee, D. Neher and Y. Zou, *Energy Environ. Sci.*, 2022, **15**, 2806–2818.
39 J. Wan, I. Dyadishchev, R. Sun, Q. Wu, Y. Wu, M. Zhang, S. Peregudova, S. Ponomarenko, Y. Luponosov and J. Min, *J. Mater. Chem. A*, 2022, **10**, 17122–17131.
40 A. C. Jakowetz, M. L. Bohm, A. Sadhanala, S. Huettner, A. Rao and R. H. Friend, *Nat. Mater.*, 2017, **16**, 551–557.
41 L. Perdigon-Toro, H. Zhang, A. Markina, J. Yuan, S. M. Hosseini, C. M. Wolff, G. Zuo, M. Stolterfoht, Y. Zou, F. Gao, D. Andrienko, S. Shoaee and D. Neher, *Adv. Mater.*, 2020, **32**, e1906763.